EPJ Web of Conferences **3**, 07010 (2010)
DOI:10.1051/epjconf/20100307010

Associated Λ/Σ^0 electroproduction with the Kaos spectrometer at MAMI

P. Achenbach[a] on behalf of the A1 Collaboration

Institut für Kernphysik, Johannes Gutenberg-Universität, J.-J.-Becherweg 45, D-55099 Mainz.

Abstract. An instrument of central importance for the strangeness photo- and electroproduction at the 1.5 GeV electron beam of the MAMI accelerator at the Institut für Kernphysik in Mainz, Germany, is the newly installed magnetic spectrometer Kaos that is operated by the A1 collaboration in $(e,e'K)$ reactions on the proton or light nuclei. Its compact design and its capability to detect negative and positive charged particles simultaneously complements the existing spectrometers. The strangeness program performed with Kaos in 2008–9 is addressing some important issues in the field of elementary kaon photo- and electroproduction reactions. Although recent measurements have been performed at Jefferson Lab, there are still a number of open problems in the interpretation of the data and the description of the elementary process using phenomenological models. With the identification of Λ and Σ^0 hyperons in the missing mass spectra from kaon production off a liquid hydrogen target it is demonstrated that the extended facility at MAMI is capable to perform strangeness electroproduction spectroscopy at low momentum transfers $Q^2 < 0.5\,(\mathrm{GeV}/c)^2$. The covered kinematics and systematic uncertainties in the cross-section extraction from the data are discussed.

1 Introduction

Analogous to the successful description of pion photoproduction in the Δ resonance region or η photoproduction in the second resonance region, phenomenological models can describe the electromagnetic kaon production amplitudes associated to Λ/Σ^0 hyperons. Many experimental data for kaon production has been collected sofar by Jefferson Lab, ELSA, SPring8, GRAAL, and Tohoku. Although recent measurements with high statistics have been performed at Jefferson Lab [1–3], there are still a number of open problems in the interpretation of the data and the description of the elementary process using phenomenological models, see Ref. [4] for a recent discussion.

Theoretical groups have developed a particular type of effective Lagrangian model, commonly referred to as isobar approach, in which the reaction amplitude is constructed from *s*-, *t*-, or *u*-channel exchange diagrams. Most of the models use single-channel approaches, in which a single hadron is exchanged. Since several resonances may contribute in this channel, models disagree on their relative importance, and many free parameters have to be fixed. Experimental set-ups used to study the strangeness production channels are missing forward angle acceptance leading to a strong variation of the models in the forward region. Concerning the data published after 1990 discrepancies between the CLAS [5] and SAPHIR [6] experiments do not allow for a unique description of the process. This situation clearly indicates that more experimental and theoretical work is needed in order to provide a comprehensive understanding of the elementary reaction. A number of new experiments are now addressing these issues, among them the charged kaon electroproduction program with the Kaos spectrometer at MAMI.

[a] e-mail: patrick@kph.uni-mainz.de

2 Kinematics and experimental setup

The accelerator facility MAMI at the Institut für Kernphysik in Mainz, Germany, can now be used to study elementary strangeness processes as the threshold energy was crossed by the 1508 MeV end-point energy of stage C compared to the 855 MeV end-point energy of stage B. The kinematic regions accessible in electroproduction by the electron accelerator facility are shown in Fig. 1.

In a typical two-arm strangeness electroproduction experiment a charged kaon is detected in coincidence with a scattered electron and the recoiling hadronic system remains unobserved. The incident electron of energy E scatters by radiating a virtual photon, q^μ. The scattered electron of energy E' is emitted at a polar angle θ with respect to the direction of the incident beam. The virtual photon carries momentum, $\mathbf{q}$, and energy, q_0, defining the momentum transfer squared $Q^2 = -q^\mu q_\mu$.

The goals of the first measurements at MAMI were to determine the angular dependence of the virtual photoproduction cross-section at very low Q^2. This cross-section may be related to the five-fold differential electroproduction cross-section via:

$$\frac{d^5\sigma}{dE'd\Omega_e d\Omega_K^*} = \Gamma_v \frac{d^2\sigma}{d\Omega_K^*}(W, Q^2, \epsilon, \theta_K^*, \phi_K^*)\,, \qquad (1)$$

where the kaon angles θ_K^* and ϕ_K^* are given in spherical coordinates in the hadronic center-of-mass system and the

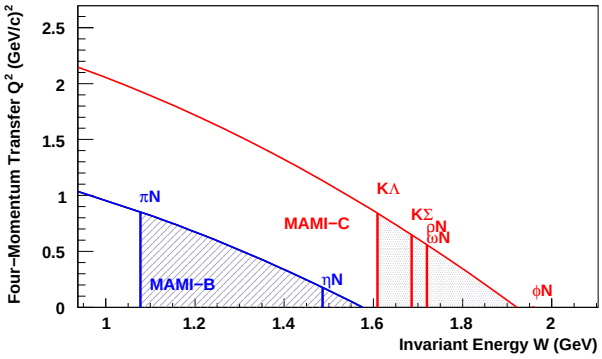

Fig. 1. Kinematic regions accessible in electroproduction by the electron accelerator facility. The end-point energy of stage MAMI-B is 855 MeV and of stage MAMI-C is 1508 MeV (as of Summer 2009). The threshold energies for $\pi/\eta/\rho/\omega$ and ϕ production off the nucleon and the associated strangeness channels $K\Lambda$ and $K\Sigma$ are indicated; the kinematic regions for pion and kaon production are shaded. Only at MAMI-C the electroproduction of open strangeness is possible.

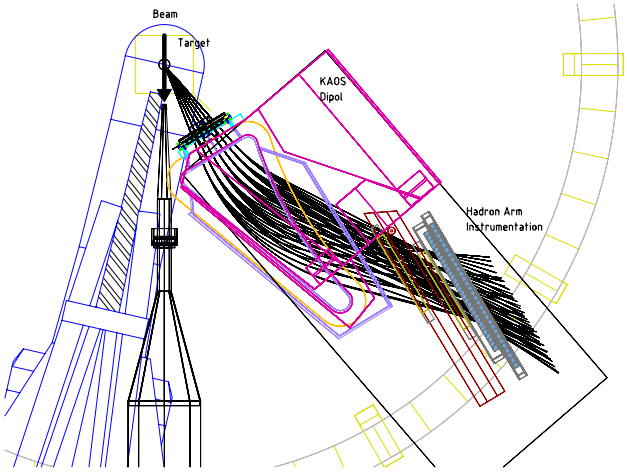

Fig. 2. Overview of the first spectrometer set-up for strangeness electroproduction at the Mainz Microtron MAMI. Ray-traced particle trajectories through the Kaos spectrometer are shown by full lines. The instrumentation of the hadron arm is indicated. Both spectrometers were positioned as close to the exit beam-line as mechanically possible.

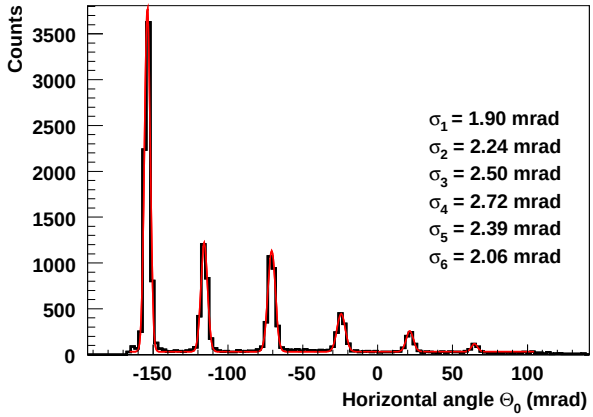

Fig. 3. Preliminary analysis of elastically scattered electrons of 450 MeV energy, back-traced from the detector system of the Kaos spectrometer to the target, before applying any corrections of the aberrations. The sieve-slit collimator was made of a 20 mm thick lead block with holes of angular width of $\sigma \sim 2.4$ mrad at 1000 mm distance to the target. The peaks in the projection on the axis of the target angle θ_0 in the dispersive plane were fitted by Gaussian distributions, resulting in widths of $\sigma \sim 1.9$–2.7 mrad.

flux factor of virtual photons per scattered electron into $dE'd\Omega_e$ is given by:

$$\Gamma_v = \frac{\alpha}{2\pi^2}\frac{E'}{E}\frac{|\mathbf{q}|}{Q^2}\frac{1}{1-\epsilon}, \qquad (2)$$

and the transverse polarization factor of the virtual photon is denoted by ϵ:

$$\epsilon = \left(1 + 2\frac{|\mathbf{q}|^2}{Q^2}\tan^2\frac{\theta}{2}\right)^{-1}. \qquad (3)$$

First strangeness production experiments were carried out at the spectrometer facility of the A1 Collaboration [7]. An instrument of central importance for this program is the newly installed magnetic spectrometer Kaos, dedicated to the detection of charged kaons. Its compact design and its capability to detect negative and positive charged particles simultaneously complements the existing spectrometers.

Fig. 2 shows a schematic drawing of the Kaos spectrometer as realized in the spectrometer hall. Kaos is operated in a single-dipole configuration. The first-order focusing is achieved with a bending of the central trajectory by $\sim 45^\circ$ with a momentum dispersion of 2.2 cm/%. The dispersion to magnification ratio of the Kaos hadron arm is $D/M_x = 1.2$ cm/% which leads to a first-order resolving power, $R_1 = D/(M_x\sigma_x)$, of 2 400 for a beam-spot size, σ_0, of 0.5 mm. The first order momentum resolution, $\Delta p/p = \sqrt{(\sigma_x^2 + M_x^2\sigma_0^2)/D^2}$, is determined from these values to be of the order of $\sim 10^{-3}$, where the spatial resolution in the focal plane, σ_x, was approximated with the anode wire distance of 2 mm in the MWPC.

Detailed measurements with electron beams elastically scattered off ^{12}C and ^{181}Ta foils have been performed to study the properties of the magnet optics. To select well determined angles in both planes a sieve collimator, made of 20 mm thick lead with 16 holes, 5 mm in diameter each, was installed in a distance of 1000 mm from the target in front of the magnet. For each hole the sieve collimator defines primary angle distributions with a width of $\sigma = 2.45$ mrad. Electrons passing different holes are clearly separated in the reconstructed coordinates. The deviations to the nominal hole coordinates quantify the uncorrected optical aberrations of the system. The magnitude of the necessary correction of the transfer matrix elements is of the order of 10 mrad or more, as can be deduced from the deviations of the measured hole positions to the nominal positions. The projections of the events to the target angle θ_o in the dispersive plane produced peaked distributions width widths of $\sigma \sim 1.9$–2.7 mrad, as shown in Fig. 3. A finer collimator was prepared in 2009 for an improved determina-

Table 1. Kinematics of the 2009 beam-time on kaon elementary electroproduction at the Mainz Microtron.

initial electron energy, E (MeV)	1508
final electron energy, E' (MeV)	327
electron scattering angle, θ (deg)	15.5
degree of transverse polarization, ϵ	0.406
total energy in *cm* system, W (MeV)	1745
virtual photon momentum transfer, Q^2 (GeV$^2/c^2$)	.036
virtual photon flux factor, Γ_v (ph./GeV/sr)	.004

tion of the transfer matrix elements. It contained 53 holes in 5 different horizontal lines along the dispersive plane. The calibrations are ongoing and no final results from the experiments can be provided unless the calibration runs are fully analyzed.

In 2008 and 2009 strangeness production off the proton was measured at two different kinematic settings with this experimental set-up. The beam from MAMI-C impinged with an energy of 1507 MeV on a liquid-hydrogen target. Positive kaons were detected in the Kaos spectrometer benefiting from the large in-plane angular acceptance at scattering angles θ_K = 21–43°, and of the large momentum acceptance at p = 400–700 MeV/c. The scattered electrons from the H($e, e'K$) reaction were detected in the high-resolution magnetic spectrometer B (SpekB) that was kept fixed at an angle of $\theta \approx$ -15° during the experiments.

The luminosity was calculated from the density and thickness of the target, and the beam current, and is corrected for the DAQ dead-time. The collected data in 2008 corresponds to effectively 3 days of beam-time at 1–4 μA beam current for each kinematic point with a total integrated luminosity of $\int \mathcal{L}dt \sim 284$ fbarn^{-1}. One setting with a central momentum in Kaos of 530 MeV/c was continued by a longer data-taking campaign on kaon elementary electroproduction in 2009 for a statistically and systematically improved data-set. In Table 1 a summary on this particular kinematics is given. The current was held constant at 2, respectively 4 μA. With a run-time of 265 h using 2 μA beam current (at 13 % dead-time) and 40 h using 4 μA beam current (at 44 % dead-time) the accumulated and corrected luminosity for the 2009 data-taking campaign was $\int \mathcal{L}dt \sim$ 3000 fbarn^{-1}.

3 Particle tracking and identification with Kaos

The tracking of particles through Kaos is performed by means of two large MWPC with a total of 2 × 310 analogue channels. Five cathode wires are connected together and are brought to one charge sensitive preamplifier followed by an ADC card. The transputer-based read-out system is connected to a multi-link card of a front-end computer. To determine the particle track the measured charge distributions are analyzed by the center-of-gravity method.

In the subsequent analysis of the data not only the particle track is used, but a large set of track quality factors. For example, the correlation that exists between the induced charge measured in one cathode plane to the induced charge of the perpendicular plane allows in many cases a correct pairing of clusters. Valid tracks are bound to angular limits, given by the acceptance of the spectrometer. Especially the relation between vertical hit positions of the two chambers provides a powerful criterion for the track finding. The multi-hit capability of the MWPC is important to allow for beam currents above 1 μA. As long as two tracks are sufficiently separated in space to induce distinct charge distributions on both cathode planes, the double track ambiguity can be resolved with high efficiency.

In 2009 two small scintillating detectors of dimensions $\sim 2 \times 3\,\mathrm{cm}^2$ with 5 mm thickness were installed in front of each MWPC to determine the tracking and detection efficiency of the hadron arm. The detectors can easily be moved out of the spectrometer's acceptance when not in use.

Particle identification in the Kaos spectrometer is based on the particle's time-of-flight and its specific energy loss. A segmented scintillator wall with 30 paddles read out at both ends by fast photomultipliers is located near the focal-surface and measures the arrival time. A second wall with 30 paddles is used to discriminate valid tracks against background events. A top–bottom mean timing for deriving the trigger is performed by summing the analogue signals. The signal amplitudes were corrected for the particle's pathlength through the scintillator bulk material and the light absorption inside the paddle. Because of aging of the material the absorption of the scintillation light inside the scintillator is strong.

The time spectrum is systematically broadened by the propagation time dispersion inside the scintillator, the time differences between different scintillator paddles and their associated electronic channels, and by the variation of the time-of-flight, being proportional to the pathlength through the spectrometer. The Gaussian width of the (e', π) peak after corrections is Δt_{FWHM} = 1.07 ns, which is a typical inter-spectrometer time resolution.

From the point of view of background events in the detectors the set-up of the Kaos spectrometer at forward angles is problematic. Shielding walls were installed comprising neutron shielding material (borated polyethylene) and lead for the electromagnetic shielding. In order to cope with the remaining high background rates Kaos has been equipped with a modern trigger system. The correlation between the paddles in both walls corresponding to valid trajectories was employed for the trigger decision. The relatively high complexity of the valid patterns and the intrinsic necessity of a flexible trigger logic for a spectrometer that faces a wide experimental program demanded a programmable logic system which was realized in so-called VUPROM modules. Each so called VME Universal Processing Module (VUPROM) has 256 I/O channels in a 1-unit-wide VME 6U form-factor. The digital signals are transmitted in high speed differential LVDS standard and are combined in 8 groups of 32 channels each, where one group is reserved for output, three groups are allocated to input, and the remaining four groups are freely configurable as input or output. Such a module is equipped with

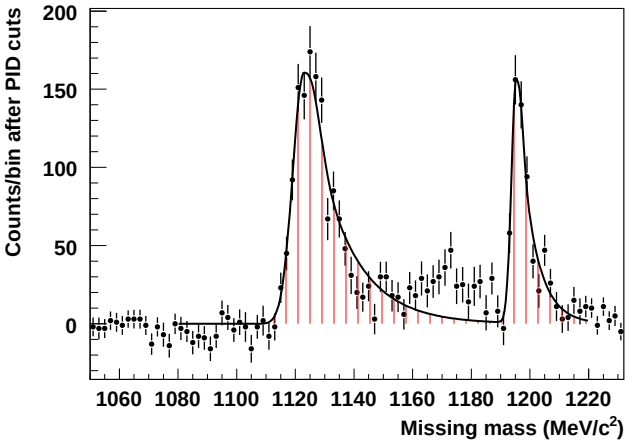

Fig. 4. Preliminary missing mass spectrum in the H$(e,e'K^+)$ reaction from the 2009 data-taking campaign as discussed in the text. The mass resolution is limited by the errors in the estimated transfer matrix that was not yet corrected for the aberrations seen in calibration measurements. The broad structure at 1170 MeV$/c^2$ is believed to be caused by particles scattered inside the spectrometer. The background in two averaged (e',K) coincidence time side-bands was subtracted with the appropriate weight.

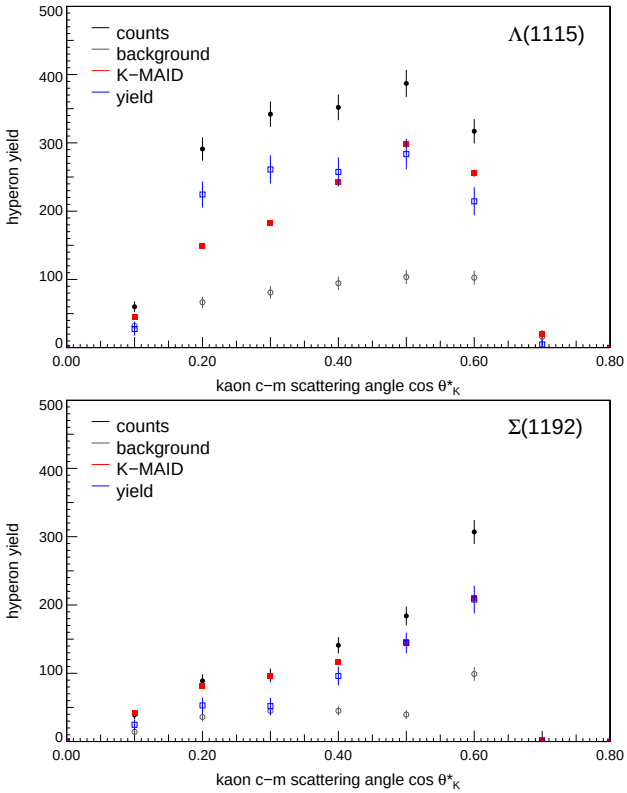

Fig. 5. Preliminary yield of identified H$(e,e'K^+)\Lambda,\Sigma^0$ reactions as a function of the center-of-mass kaon scattering angle. The measured events (open round symbols) are corrected for background events (black round symbols) to obtain the hyperon yield (blue round symbols). The data is compared to a Monte Carlo simulation using the K-Maid model [10] as an input for the cross-sections and a generalized acceptance function for the detector description. The background subtraction is still dependent on the calibration.

one VIRTEX-4 FPGA, capable of operation at 400 MHz, and one 1 GHz DSP. The coincidence trigger is based on time-of-flight and is therefore generated from the VUPROM logic and from SpekB scintillator signals.

Some more selected properties of the optics of the KAOS spectrometer, its kaon identification capabilities, and existing or planned modifications to operate KAOS as a double-arm spectrometer under zero degree scattering angle can be found in Ref. [8].

4 Data analysis

Kaon identification is based on specific energy-loss and time-of-flight, electron identification on a signal in a gas Cherenkov counter. The flight time difference between protons and kaons is 10–15 ns, between pions and kaons 5–10 ns. The energy-loss separation between kaons and pions is small, whereas the separation between kaons and protons is of the order of 2–5 MeV$/$cm. The following cuts were applied to a limited data set taken with 2 μA beam current in 2009:

Electron identification: Finite sum of Cherenkov counter amplitudes to reject pions in the electron arm.

Spectrometer fiducial volume: $\theta_0 >$ -10.5 ° and $\theta_0 <$ 8° and $\theta_0 < 0.475 \times (\Delta p + 20\,\%)$ to restrict the acceptance to a region where agreement between the Monte Carlo code and the analyzed data was excellent.

MWPC track reconstruction: MWPC quality > 0.0001 ensuring good quality tracks in the hadron arm.

Particle identification: Positive squared missing mass for a proper missing mass reconstruction, and $p_{Kaos} < 1.8 \times p_{central}$ for a proper momentum reconstruction, and $\beta_{Kaos} > 0.4$ to reject erroneous timing values.

Kaon identification: $|t^K_{F,G}| < 1.8$ ns, being the measured TOF corrected for the expected kaon flight time, and $|\Delta E^K_{F,G}| < 400$ keV, being the measured specific energy loss corrected for the expected kaon energy loss. A small t^K indicates that the correct mass hypothesis has been made while a small ΔE^K reduces the random background events.

Reaction channel identification: For the Λ and Σ^0 hyperons 1110 MeV$/c^2 < M_X <$ 1140 MeV$/c^2$, respectively 1190 MeV$/c^2 < M_X <$ 1205 MeV$/c^2$.

After electron and kaon identification the measured momenta, in magnitude and direction with respect to the incoming beam, allow for a full reconstruction of the missing energy and missing momentum of the recoiling system. After application of all cuts on the data, the remaining events are used to extract the kaon yield in the two hyperon channels. A cut was placed on the missing mass in order to separate the Λ and Σ^0 reaction channels. Because the Σ^0 peak resides on the tail of the Λ peak, the latter has to be accounted for in the analysis of the Σ^0-region of the measured spectrum. A preliminary missing mass distribution is shown in Fig. 4. The mass resolution is limited by the

errors in the estimated transfer matrix that was not yet corrected by the aberrations seen in calibration measurements. Since the Kaos spectrometer is operated as a single dipole with open yoke geometry a significant fraction of detected particles have scattered inside the spectrometer and need to be treated accordingly.

Random background events in the missing mass spectra were subtracted by two averaged (e', K) coincidence time side-bands with the appropriate weights. The preliminary yields of identified $\mathrm{H}(e, e'K^+)\Lambda, \Sigma^0$ reactions as a function of the center-of-mass kaon scattering angle are shown in Fig. 5. The background subtraction is still dependent on the calibration. The data is compared to a Monte Carlo simulation using the K-Maid model [10] as an input for the cross-sections and a generalized acceptance function for the detector description.

The number of kaons that were actually detected was less than the true number of kaons produced in the reaction, and corrections for their decay had to be taken into account. The kaon survival fraction varied between 0.2 and 0.35 for the range of momenta detected.

5 Extraction of cross-sections

The further analysis required a detailed Monte Carlo simulation of the experiment in order to extract cross-section information from the data. The experimental yield can be related to the cross-section by

$$Y = \mathcal{L} \times \int \Gamma(Q^2, W) \frac{d^2\sigma}{d\Omega_K^*} A(d^5V) R(d^5V)\, dQ^2 dW d\phi_e d\Omega_K^* , \tag{4}$$

where $\mathcal{L}$ is the experimental luminosity including global efficiencies such as dead-times, A is the acceptance function of the coincidence spectrometer set-up including momentum dependent corrections such as the tracking efficiency, and R is the correction due to radiative or energy losses.

In the Monte Carlo for the integral is evaluated in the phase-space $\Delta V = \Delta Q^2 \Delta W \Delta\phi_e \Delta\Omega_K^*$ with limits that extended beyond the physical acceptances of the spectrometers. The simulation is giving the phase-space accepted by the spectrometers according to a chosen kinematics together with the radiative corrections, absorption and decay losses as well as detector inefficiencies. By virtue of the Monte Carlo technique used to perform this integral the quantities A and R are not available separately or on an event-by-event basis. In Fig. 6 the phase-space in the target angle vs. momentum plane for kaon acceptance in the Kaos spectrometer simulated by a Monte Carlo integration method is compared to the data measured during the 2009 beam-time. The kaon data was extracted after particle identification and missing mass cuts. The agreement inside the fiducial volume is excellent.

The general acceptance can be written in terms of the cross-section at a given point $(d^2\sigma/d\Omega_K^*)_{0,\theta_K^*}$, called the scaling point, at $\langle Q^2 \rangle$, $\langle W \rangle$, $\langle \phi_e \rangle$, and $\langle \phi_K^* \rangle$, when studying

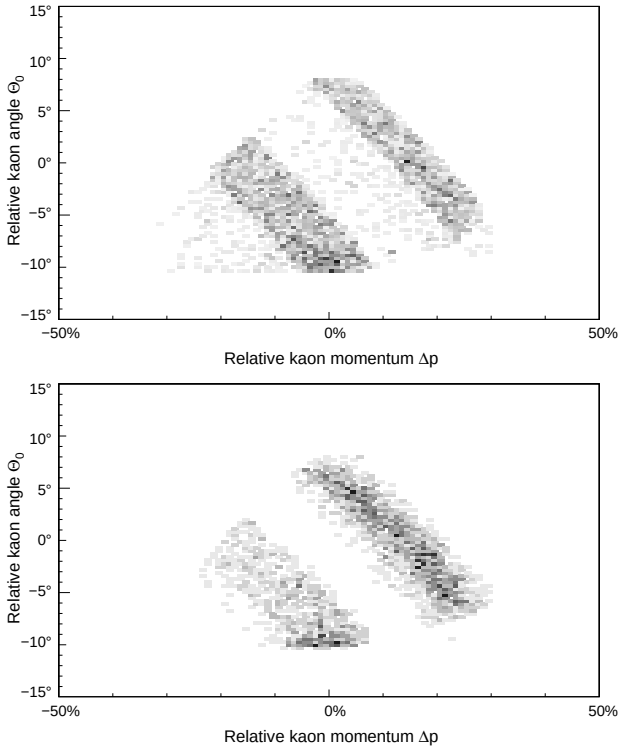

Fig. 6. Phase-space in the target angle vs. momentum plane for kaon acceptance in the Kaos spectrometer simulated by a Geant4 Monte Carlo integration (top) and measured during the 2009 beam-time (bottom). The kaon data was extracted after particle identification and missing mass cuts. The simulation includes radiative corrections and energy-loss in the target.

the dependence on the remaining variable $\cos\theta_K^*$:

$$Y = \mathcal{L} \times \left(\frac{d^2\sigma}{d\Omega_K^*}\right)_{0,\theta_K^*} \times \int \Gamma(Q^2, W) \frac{\frac{d^2\sigma}{d\Omega_K^*}}{\left(\frac{d^2\sigma}{d\Omega_K^*}\right)_{0,\theta_K^*}} A(d^5V) R(d^5V)\, dQ^2 dW d\phi_e d\Omega_K^* \tag{5}$$

Then, the behavior of the cross-section across the acceptance needs to be implemented according to a given theoretical description. We applied the K-Maid [10] isobar model, however, we could as well compare to the full (SL) and the simplified version (SLA) of the so-called Saclay-Lyon model [9]. The scaling point for the data set from 2009 is at $\langle Q^2 \rangle = 0.036\,(\mathrm{GeV}/c)^2$, $\langle W \rangle = 1.750\,\mathrm{GeV}$, $\langle \epsilon \rangle = 0.4$. Finally, the cross-section is evaluated dividing the yield by the luminosity and the evaluated integral. An important observable to be investigated is the stability of the results as a function of the applied cuts and its influence on the extracted cross-section. Up to now, systematic uncertainties being discussed in the next section hinder the extraction of final values.

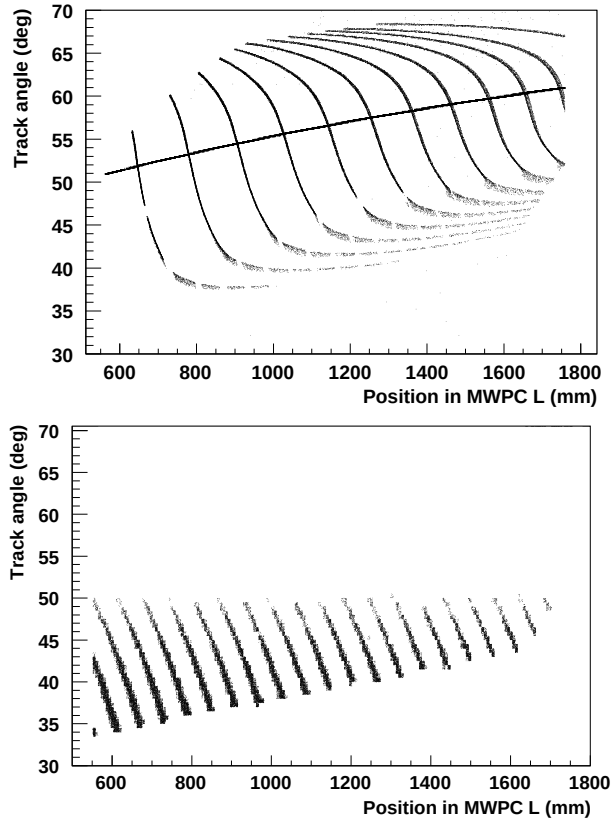

Fig. 7. Top: Projection of simulated tracks for particles with momenta of 350 MeV up to 600 MeV in steps of 25 MeV, over the full angular acceptance, and for particles of central target angles over the full momentum acceptance, in the coordinate system of the tracking chambers. In the regions with strong curvature the momentum depends on many higher-order terms of the transfer matrix. Bottom: Simulated geometrical scintillator wall inefficiencies in the same coordinate system. Both effects contribute to systematic uncertainties in the cross-section extraction.

6 Systematic uncertainties

The total efficiency for the detection of kaons with the Kaos spectrometer can be factored into the intrinsic wire chamber (MWPC) detection efficiency, the analysis cut efficiency, the trigger efficiency, and the tracking efficiency. In order to investigate the MWPC, tracking, and trigger efficiencies dedicated measurements have been performed in 2008 and 2009. The efficiency of the MWPC for the identification of minimum ionizing particles is measured to be better 98 % with only small variations over time. On the contrast, the tracking efficiency is dependent on the hit multiplicities in the wire chambers leading to ghost tracks that are classified according to a likelihood method and that are matched to scintillator hits. The track reconstruction in the wire chambers represents a primary source of inefficiency for beam currents of several μA. For pions tracking efficiencies ranged between 76 and 45 % corresponding to beam currents of 1–4 μA, for protons the efficiencies were between 92 and 77 %.

In an ideal spectrometer the position along the focal surface at which a particle is detected is directly related to its momentum. In practice, however, due to kinematic broadening and spectrometer aberrations this position will also depend on the angle of the particle trajectory with the central ray. Fig. 7 (top) shows the projection of simulated tracks with momenta of 350 MeV up to 600 MeV over the full angular acceptance in the coordinate system of the tracking chambers. Particles with given momenta but varying target angles leave traces in this coordinate system that are lines of constant slopes in the central region of the acceptance and are strongly curved at the edges. The plot includes also the trace for particles of central target angles over the full momentum acceptance. In the regions with strong curvature the momentum depends on many higher-order terms of the transfer matrix, which need to be precisely determined.

The trigger was generated by a combination of hits in the two scintillator walls. Particular momentum and track angle combinations allow the particle to cross the gaps between the scintillator paddles giving rise to significant detector inefficiencies. In Fig. 7 (bottom) a simulation of these geometrical inefficiencies are shown in the tracking coordinate system. Momentum and track angle dependent trigger efficiency corrections need to be applied to the generalized acceptance.

7 Summary

Using the recently installed magnetic spectrometer Kaos and a high-resolution spectrometer in coincidence it was possible to measure elementary kaon electroproduction at MAMI in a kinematic regime sofar not covered by Jefferson Lab experiments. At different settings we have confirmed the particle identification power and tracking capabilities of the Kaos spectrometer's hadron arm detection system. The large background rates and inefficiencies encountered in the 2008–9 data-taking campaigns are corrected using dedicated calibration data and simulation procedures. The systematic uncertainties in the cross-section extraction are under study.

References

1. R. M. Mohring *et al.* (E93-018 Collaboration), Phys. Rev. **C 67**, (2003) 0552025.
2. D. S. Carman *et al.* (CLAS Collaboration), Phys. Rev. Lett. **90**, (2003) 131804.
3. P. Ambrozewicz *et al.* (CLAS Collaboration), Phys. Rev. **C 75**, (2007) 045203.
4. T. Mart, *Proc. Intern. Symposium on Strangeness in Nuclear and Hadronic Systems (Sendai08)* (eds. K. Maeda *et al.*, Sendai, Japan, 2008), 51.
5. K. H. Glander *et al.* (SAPHIR Collaboration), Eur. Phys. J. **A 19**, (2004) 251.
6. R. Bradford *et al.* (CLAS Collaboration), Phys. Rev. **C 73**, (2006) 035202.

7. K. I. Blomqvist *et al.* (A1 Collaboration), Nucl. Instr. Meth. Phys. Res. **A 403**, (1998) 263.
8. P. Achenbach, *Proc. Intern. Symposium on Strangeness in Nuclear and Hadronic Systems (Sendai08)* (eds. K. Maeda *et al.*, Sendai, Japan, 2008), 332.
9. T. Mizutani, C. Fayard, G.-H. Lamot, and B. Saghai, Phys. Rev. **C 58**, (1998) 75.
10. T. Mart and C. Bennhold, Phys. Rev. **C 61**, (1999) 012201(R); http://www.kph.uni-mainz.de/MAID/